Available online at www.sciencedirect.com
ScienceDirect
International Journal of Heat and Fluid Flow 28 (2007) 469–482
International Journal of HEAT AND FLUID FLOW
www.elsevier.com/locate/ijhff

Natural convection air-cooling of a substrate-mounted protruding heat source in a stack of parallel boards

Gilles Desrayaud [a,b,*], Alberto Fichera [c], Guy Lauriat [a,d]

[a] LETEM, Laboratoire d'Etude des Transferts d'Energie et de Matière, France
[b] INSSET, Université de Picardie Jules Verne, 48 rue Raspail BP 422, 02109 Saint-Quentin Cedex, France
[c] Istituto Fisica Tecnica, Università di Catania, Viale A. Doria 6, 95125 Catania, Italy
[d] Université de Marne-la-Vallée, Cité Descartes, Bât. Lavoisier, Champs-sur-Marne, 77454 Marne-la-Vallée, France

Accepted 3 July 2006
Available online 29 September 2006

Abstract

The problem numerically investigated is that of steady, two-dimensional laminar natural convection in a system of parallel vertical channels with a single protruding heat module mounted mid-height on a substrate of finite-thickness. The input heat flux at the base of the module is removed through the module to the flow by convection and through the substrate by conduction. The system simulates cooling passages in a stack of printed circuit boards (PCB) with heat modules attached on the surface of one board. Heat transfer from both sides of the boards is taken into account. The solution is computed simultaneously in the solid (module and substrate) and in the fluid regions taking into account the continuity of the temperature and heat flux at the solid–fluid interfaces. The objective of this work is to determine heat transfer and fluid flow characteristics. A parametric study was conducted by varying the thermal conductivity and the thickness of the substrate and the width of the module. A variation in the substrate conductivity considerably affects the module temperature while the flow structure is only slightly altered. It is demonstrated that streamwise conduction through the substrate is an important cooling mechanism and must be accounted for.

Keywords: Electronic air-cooling; Natural convection; Conjugate heat transfer; Heat source; Numerical study

1. Introduction

This study involves air-cooling of single chip components on a stack of printed circuit boards (PCB). Natural convective air-cooling is still the preferred choice in the cooling of electronic equipment even if it is reserved to low heat generating devices. This is due to its simplicity in design, availability, low cost and ease of maintenance. Moreover, it is noise- and vibration-free and highly reliable, which is essential for domestic applications. A comprehensive review of convective cooling options in electronic packages was provided by Sathe and Sammakia (1998).

Convective cooling of electronic components mounted on circuit boards has been the subject of a large number of papers during the last decade. This interest was motivated by the rapid advances in electronic technology with the trends of the electronic industry being reduction in size. Relatively to natural convective cooling of protruding sources, almost all the studies are in single channel with no-thickness substrate. Habchi and Acharya (1986) dealt with the laminar mixed convection in a partially blocked vertical channel, symmetrically or asymmetrically heated, the smooth surface being adiabatic. For both cases, they found that the Nusselt numbers are smaller than the corresponding smooth duct Nusselt numbers. Hung and Shiau (1988) performed experiments of natural convection in

* Corresponding author. Address: INSSET, Université de Picardie Jules Verne, 48 rue Raspail BP 422, 02109 Saint-Quentin Cedex, France. Tel.: +33 3 23 62 89 59; fax: +33 3 23 62 89 35.
E-mail address: gilles.desrayaud@insset.u-picardie.fr (G. Desrayaud).

0142-727X/$ - see front matter © 2006 Elsevier Inc. All rights reserved.
doi:10.1016/j.ijheatfluidflow.2006.07.003

Nomenclature

A	aspect ratio of the channel ($A = \ell/b$)
b	channel opening
g	gravitational acceleration
h	module length
H	dimensionless module length ($H = h/b$)
K	dimensionless parameter in momentum equation
ℓ	channel height
$\dot{M}$	dimensionless mass flow rate
p	dimensional static pressure
P_m	dimensionless motion pressure
Pr	Prandtl number ($Pr = \nu/\alpha$)
q''	dimensional input heat flux at the base of the module
Q	dimensionless local heat flux (Eq. (8))
$\bar{Q}$	dimensionless mean heat flux
R	thermal resistance
Ra	Rayleigh number ($Ra = g\beta q'' b^4/\alpha\nu\kappa_a$)
Ra^*	channel Rayleigh number ($Ra^* = Ra/A$)
s	substrate thickness
S	dimensionless substrate thickness ($S = s/b$)
T_0	ambient temperature
X, Y	dimensionless coordinates (X, $Y = x/b$, y/b)
U, V	dimensionless velocity components in X and Y directions
w	module width
W	dimensionless module width ($W = w/b$)

Greek symbols

α	thermal diffusivity
β	volumetric coefficient of thermal expansion
κ	thermal conductivity
θ	dimensionless temperature ($\theta = (T - T_0)/\Delta T$)
ρ	density of the fluid
ν	kinematic viscosity of the fluid
ξ	dimensionless coordinate contour distance along the solid–fluid interface
Λ	thermal conductivity ratio, ($\Lambda = \kappa/\kappa_a$)
ΔT	temperature difference reference ($\Delta T = q'' b/\kappa_a$)

Subscripts

a	air
above	downstream substrate (above the module)
back	back face of the substrate
below	upstream substrate (below the module)
front	front face of the substrate
m	module
s	substrate

Superscript

–	mean value

vertical parallel plates mounted with a 2D rectangular rib under asymmetric isoflux heating. They concluded that the channel spacing has no significant effect on average heat transfer performance if convective heat flux is maintained constant, but their experimental set-up had low aspect ratios, $1.4 \leqslant A \leqslant 5.6$. They observed that the existence of a protruding rib originates a turbulence zone in the downstream region. In the recirculation zone, which appears immediately downstream from the protruding rib, the heat transfer coefficients are lower than those in any other region. Said and Krane (1990) performed a numerical and experimental investigation of natural convection in an isothermal channel with a single rounded obstacle. Owing to the presence of the obstacle, the reduction of the average Nusselt number can reach 40% for a low channel Rayleigh number, i.e., $Ra^* = 10$, while it is only 5% at $Ra^* = 10^4$. They also showed that the location of the rib along the wall affects the rate of heat transfer. Lin and Hsieh (1990) presented natural convective flows, assisting and opposing, in vertical channels with asymmetrically discrete heated ribs. They reported that the flow separation/recirculation is one of the major factors influencing the temperature of the heated ribs. They found that the assisting flow is laminar and that the average Nusselt number correlation of Wirtz and Stutzman (1982) for natural convection between vertical smooth plates with symmetric heating predicts their experimental data with an average error below 2% (correlated in terms of Ra^*). Tanda (1997) experimentally investigated natural convection in a channel formed by an isothermal ribbed surface (with 5 ribs) and an opposing adiabatic smooth surface. He determined a global mean Nusselt correlation as $\overline{Nu} = f(Ra)$ showing that the heat transfer in a ribbed channel is of lesser importance than that in a smooth channel. It seems that this decrease comes from the reduction of the mass flow rate inside the channel due to the obstacles. On the other hand, an experimental study on natural convection from five rectangular grooves on a vertical isothermal plate has been reported by Kwak and Song (1998). They experimentally and numerically demonstrated that for a high Rayleigh number (based on the length of a pitch) the heat transfer rate is greater than that for a smooth surface, even if secondary recirculation is usually found in the groove and prevents the main stream from flowing into the groove. In this case, the mass flow rate is not constrained by a shrouding plate as in a channel with surface-mounted protrusions. Composite correlation on natural convection in a vertical channel with a single surface-mounted heated obstacle has been recently proposed by Desrayaud and Fichera (2003).

Studies for forced or mixed flow convection in parallel plates with substrate-mounted protruding heated sources are reviewed in the following because they were the first, and to our best knowledge only one study of this kind is available for natural convection. Davalath and Bayazitoglu (1987) were among the first to examine numerically the forced convection between parallel plates with three rectangular blocks uniformly heated. They studied conjugate conduction through the PC boards coupled to the fluid flow and the block using symmetric boundary conditions to restrict the computational domain to a single channel. Mean Nusselt number correlation was presented for different Reynolds and Prandtl numbers with and without insulated plates. Kim et al. (1992) extended the previous study to mixed convection heat transfer inside horizontally- and vertically-oriented channels. They used periodic or repeated conditions in the cross-stream direction imposed on successive base plates to isolate a single channel as computational domain. They also demonstrated that such oversimplified assumptions as isothermal or adiabatic surface wall conditions may not be entirely appropriate for simulating the cooling of electronic devices. Kim and Anand (1994) also studied such a configuration with five periodically surface-mounted heat generating blocks but with alternative boundary conditions for the temperature field at the boundary exit. They numerically determined a generalized correlation in terms of independent parameters for the thermal resistance in developing laminar flow. Periodically fully developed flow in a ribbed channel has recently been studied by Furukawa and Yang (2003) with a special attention to the thermal contact resistance between the chip and the board which has a considerable impact on thermal performance.

Although a number of papers have been published in the general area of natural convection in single channel, multiple channels with substrate effect have received only few attention, Kim et al. (1991), Fujii et al. (1994), Floryan and Novak (1995), Behnia et al. (1998). All of these authors considered the effects of wall conduction on natural convection heat transfer in vertical smooth channels uniformly or discretely heated but none investigated the problem of protruding heat sources. To our best knowledge, only one paper dealt with multiple channels with finite-thickness and protruding heat sources. The experimental and numerical work of Fujii et al. (1996) is devoted to natural convection heat transfer to air from an array of vertical parallel plates with eighteen protruding heat sources. They considered two kinds of heating conditions, uniform heat generation and concentrated heat generation within a very small volume in each source. Owing to the large number of discrete heat sources, the geometry resembles that of a smooth channel with restricted area. Therefore, the Nusselt correlation established by Fujii et al. (1994) for smooth channel is only slightly modified to take into account the protrusion effect; see also Lin and Hsieh (1990) for a similar conclusion about the Nusselt number. The numerical results of Fujii et al. (1996) agreed well with their experimental data, except for the largest aspect ratio ($A = 30$).

The above literature review indicates that the fluid flow and heat transfer adjacent to protruding heat sources has been studied primarily for mixed or natural convection in single channel or for the limiting geometrical conditions of natural convection in smooth channels. It appears also from the literature that investigations on repeated channels are somewhat scarce especially for natural convection cooling. The present investigation differs from that of Fujii et al. (1996) in the following ways: (1) parallel conducting circuit boards of finite-thickness (the substrate) with a single protruding heat source (the module) mounted mid-height on one surface of the boards is numerically studied, thus the effect of this single heated protrusion on the fluid flow and heat transfer may be scrutinized, and (2) conduction heat transfer through the substrate, which can be convected upstream or downstream of the heat source to the same channel or convected in the adjacent channel, is examined for various values of the conductivity and of the thickness of the substrate. The effect of the size of the protruding module is also studied. Therefore, the purpose of the present parametric study is to determine general trends associated with conducting substrate and protruding heat sources inside vertical open parallel channels.

2. Analysis

The physical geometry considered here is that of laminar two-dimensional natural convective air-cooling between conducting parallel plates with a single protruding heat source mounted on one side of each finite-thickness board. The boards are cooled at both the front and back surfaces

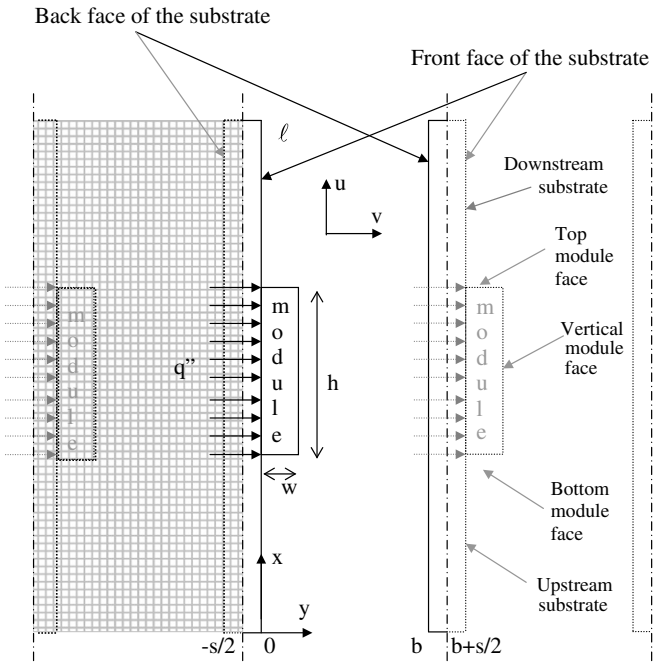

Fig. 1. Coordinate system, computational domain and surface definitions.

by the buoyancy-induced flow in the vertical direction. Since the heated modules are placed on one side of the channel surface, one may define each channel enclosed by the mid-planes of two adjacent boards. A schematic sketch of the configuration is shown in Fig. 1. The vertical boards have a length ℓ and the opening of the channels is b. Hence, the aspect ratio of the channel is $A = \ell/b$. The thickness of the boards being s, the total width of a channel is thus $(s + b)$. The height h and the width w are the dimensions of the module mounted mid-height on the board. The heat flux q'' dissipated at the base of the protruding module simulates chip operating conditions. The air at the ambient temperature T_0 enters at the bottom of the stack and proceeds upward.

2.1. Governing equations

The equations governing the flow and temperature fields are the conservation of mass, momentum and energy for an incompressible Newtonian fluid. The two-dimensional flow inside the channels is assumed steady, laminar and of constant thermal properties at the ambient temperature T_0, except for density in the buoyancy term (Boussinesq approximation). By using the hydrostatic fundamental relation for the atmospheric pressure at the outside of the channel we can write,

$$\frac{\mathrm{d}p_{\mathrm{atm}}}{\mathrm{d}x} + \rho_0 g = 0.$$

The motion pressure p_{m} in the x-momentum equation being also given by the difference between the pressure inside the channel and the pressure outside at the same elevation, it follows that $p_{\mathrm{m}} = p + \rho_0 g x = p - p_{\mathrm{atm}}$, which is usually called the pressure defect.

The following variables and quantities are used to non-dimensionalize the governing equations and boundary conditions:

$$X = x/b, \quad Y = y/b, \quad U = u/U_0, \quad V = v/U_0,$$
$$\theta = (T - T_0)/\Delta T, \quad \text{and} \quad P_{\mathrm{m}} = p_{\mathrm{m}}/\rho_0 U_0^2$$
$$= (p + \rho_0 g x)/\rho_0 U_0^2, \quad \text{where} \quad U_0 = \alpha/b \quad \text{and}$$
$$\Delta T = q'' b/\kappa_{\mathrm{a}}.$$

Then the dimensionless system of governing equations to be solved can be expressed as:

$$\frac{\partial U}{\partial X} + \frac{\partial V}{\partial Y} = 0 \tag{1}$$

$$\frac{\partial (UU)}{\partial X} + \frac{\partial (VU)}{\partial Y} + KU = -\frac{\partial P_{\mathrm{m}}}{\partial X} + Pr\left(\frac{\partial^2 U}{\partial X^2} + \frac{\partial^2 U}{\partial Y^2}\right) + Ra\,Pr\,\theta \tag{2a}$$

$$\frac{\partial (UV)}{\partial X} + \frac{\partial (VV)}{\partial Y} + KV = -\frac{\partial P_{\mathrm{m}}}{\partial Y} + Pr\left(\frac{\partial^2 V}{\partial X^2} + \frac{\partial^2 V}{\partial Y^2}\right) \tag{2b}$$

$$\frac{\partial (U\theta)}{\partial X} + \frac{\partial (V\theta)}{\partial Y} = \left(\frac{\partial}{\partial X}\left(\Lambda \frac{\partial \theta}{\partial X}\right) + \frac{\partial}{\partial Y}\left(\Lambda \frac{\partial \theta}{\partial Y}\right)\right). \tag{3}$$

The three dimensionless numbers appearing in the governing equations are:

- the Rayleigh and Prandtl numbers $Ra = \dfrac{g\beta\Delta T b^3}{\alpha\nu}$, $Pr = \dfrac{\nu}{\alpha}$,
- the thermal conductivity ratio $\Lambda = \kappa\,/\kappa_{\mathrm{a}}$, equal to Λ_{s} in the substrate and to Λ_{m} in the module.

The dimensionless K-parameter is introduced in the momentum equations because the computational domain encompasses the solid parts (substrate and module) for which the K-parameter is fixed at a very high value ($K > 10^{20}$) while its value is very low within the fluid part ($K < 10^{-20}$).

The flow being restricted to the channel, appropriate boundary conditions are required at the open bottom and top. Referring to Fig. 1, the boundary conditions can be summarized as follows:

$$\text{Inlet}: \quad 0 \leqslant Y \leqslant 1 \ \text{and} \ X = 0: \quad \frac{\partial U}{\partial X} = 0,$$
$$V = 0, \ \theta = 0, \ P_{\mathrm{m}} = -\frac{\dot{M}^2}{2}. \tag{4}$$

$$\text{Outlet}: \quad 0 \leqslant Y \leqslant 1 \ \text{and} \ X = A: \quad \frac{\partial U}{\partial X} = \frac{\partial V}{\partial X} = 0,$$
$$P_{\mathrm{m}} = 0; \quad \text{if} \ U \geqslant 0 \ \frac{\partial \theta}{\partial X} = 0 \quad \text{otherwise} \ \theta = 0. \tag{5}$$

$$\text{Base of the module}: \quad \frac{A}{2} - \frac{H}{2} \leqslant X \leqslant \frac{A}{2} + \frac{H}{2}$$
$$\text{and} \ Y = 0: \quad -\Lambda_{\mathrm{m}} \frac{\partial \theta}{\partial Y} = 1. \tag{6}$$

The dimensionless mass flow rate is calculated as $\dot{M} = \int_0^1 U|_X \mathrm{d}Y$.

In the so-called developing flow regime, any region outside the channel can be neglected because the fluid is not pre-heated before entering. Therefore, the computational domain can be restricted to the channel. The Bernoulli equation indicates that the mass flow rate depends on the square root of the difference between the ambient pressure and the pressure at the inlet (Eq. (4)). The importance of the inlet pressure boundary condition for properly capturing outlet flow reversal has recently been demonstrated numerically by Marcondes and Maliska (1999). At the outflow boundary, the transport was assumed to be locally parabolic, i.e., gradients of velocity and temperature were assumed to be approximately zero while the pressure is assumed to be equal to the ambient pressure (Eq. (5)). No significant differences in the flow and temperature fields were found if for U-velocity we use the conservation of mass instead of zero gradient. The fluid entering through the outlet section of the channel (with downward velocity) is at the ambient temperature. Zamora and Hernandez (1997) demonstrated that these types of boundary condition are able to capture outlet recirculation flows (see also Desrayaud et al., 2002 and Desrayaud and Fichera, 2003).

To simulate thermal coupling between two adjacent channels, the repeated nature of the channels allows the employment of the following periodic thermal conditions (Kim et al., 1992, Fujii et al., 1996, Behnia et al., 1998, Furukawa and Yang, 2003) with the symmetry plane at the substrate middle plane:

$$\text{Multiple channels:}\quad 0 \leqslant X \leqslant A: \quad \theta|_{Y=-S/2} = \theta|_{Y=1+S/2} \text{ and } \left.\frac{\partial\theta}{\partial Y}\right|_{Y=-S/2} = \left.\frac{\partial\theta}{\partial Y}\right|_{Y=1+S/2}. \tag{7a}$$

In the limiting case of a single channel and its isolated shrouding plate (i.e., adiabatic B.C. at the left and right outer surfaces), the following boundary conditions are used:

$$\text{Single channel:}\quad 0 \leqslant X \leqslant A \text{ and } Y = -S \text{ or } 1: \quad \frac{\partial\theta}{\partial Y} = 0. \tag{7b}$$

In both cases, the substrate in the streamwise direction is treated as insulated at the edges

$$\text{End edges of the board:}\quad -S \leqslant Y \leqslant 0 \text{ and } X = 0 \text{ or } A: \quad \frac{\partial\theta}{\partial X} = 0. \tag{7c}$$

Since the use of a Nusselt number is not very convenient in such a conjugate problem, it is more appropriate to discuss the results in terms of heat fluxes. The dimensionless local heat flux at the solid–fluid interfaces is obtained as:

$$Q = -\Lambda_i \left(\frac{\partial\theta}{\partial n}\right)_i. \tag{8}$$

where subscript i is either s or m depending upon whether the interface is a substrate–fluid or a module–fluid interface, respectively. The dimensionless temperature gradient in the direction normal to the surface is evaluated on the solid side of the interface, **n** being the unit outward normal vector to the solid surface. The heat flux is positive when heat transfer is from the solid to the fluid, negative otherwise. The mean heat fluxes are calculated by integrating the local heat fluxes along each of the surfaces.

An overall energy balance was computed as the difference between the input heat flux at the base of the module and the net energy loss through the openings of the channel, inlet and outlet. As a result of the non-dimensionalization, the balance equation is:

$$\begin{aligned}\overline{Q} &= (\overline{Q}_{\text{below}} + \overline{Q}_{\text{m}} + \overline{Q}_{\text{above}})_{Y=0} - \overline{Q}|_{Y=1} \\ &= \int_0^1 \left.\frac{\partial\theta}{\partial X}\right|_{\text{inlet}} \mathrm{d}Y + \int_0^1 \left.\left(-\frac{\partial\theta}{\partial X} + U\theta\right)\right|_{\text{outlet}} \mathrm{d}Y \\ &\text{with}\quad \overline{Q} = \frac{q'' h}{\kappa_{\text{a}} \Delta T} = H.\end{aligned} \tag{9}$$

The input heat flux $\overline{Q}$ at the base of the module is conducted through both faces of the substrate and module surfaces. The heat flux convected inside the studied channel through the front face of the substrate ($Y = 0$) is decomposed as below, at and above the module ($\overline{Q}_{\text{below}}, \overline{Q}_{\text{m}}, \overline{Q}_{\text{above}}$) while that through the back face ($Y = 1$) is $\overline{Q}|_{Y=1}$. Owing to the channel periodicity, this heat flux is also the heat flux convected through the back face of the adjacent left channel ($Y = -S/2$), $\overline{Q}_{\text{back}}$.

From the above mathematical model, it can be seen that the problem formulation depends on eight dimensionless parameters: the Rayleigh number (Ra), the Prandtl number (Pr), the dimensions of the module ($W = w/b$, $H = h/b$), the board thickness ($S = s/b$), the aspect ratio of the channel ($A = \ell/b$) and the solid-to-fluid thermal conductivity ratios ($\Lambda_{\text{s}} = \kappa_{\text{s}}/\kappa_{\text{a}}$ and $\Lambda_{\text{m}} = \kappa_{\text{m}}/\kappa_{\text{a}}$). However, it should be noted here that, as in many previous studies for smooth open channels, the modified or channel Rayleigh number, $Ra^* = Ra/A$, is used in the following instead of the Rayleigh number.

2.2. Numerical procedure

A finite volume-based single-domain approach using the SIMPLER algorithm described by Patankar (1980) is used to solve the system of elliptic partial differential equations for the velocity, pressure and temperature. In materials that are solid (e.g., module, substrate) a large value of the K-parameter is prescribed. Thus the same momentum equation Eq. (2) was solved throughout the computational domain. Boundary conditions (heat flux, temperature, velocities) at surfaces within the domain are ensured by using the harmonic mean for the interface parameters, conductivities and K. The conditions expressing the continuity of heat flux and the temperature equality at the solid–fluid interface are thus implicitly satisfied in the present formulation. The governing equations were cast in transient form and the time integration was performed by using the Alternating Direction Implicit algorithm. The Poisson equations of the pressure and of the pressure correction were also solved by employing the ADI scheme. Since we are interested by the steady-state solutions only, the false transient method of Mallison and de Vahl Davis (1973) was employed.

The governing transport equations along with the boundary conditions listed above were solved using a Cartesian grid structure covering the entire domain of interest, solid as well as fluid regions. The grid-structure was non-uniform in nature and distributed over the fluid and solid regions to capture steep velocity, pressure, and temperature gradients due to the presence of the heating module. Grid nodes were finely spaced near the solid–fluid interfaces where field variables changed rapidly, and coarsely farther away from the interfaces.

Validation of the numerical procedure was made by performing calculations for the case of laminar flow in a vertical smooth channel because experimental and numerical results are available in the archival literature. Fig. 2 compares the results of the present work with those of Ramanathan and Kumar (1991) and Rohsenow et al. (1998) involving natural convection in a vertical smooth channel

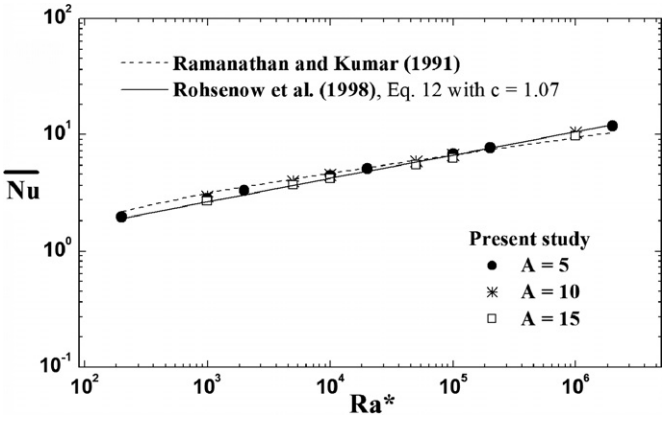

Fig. 2. Comparison of the mean Nusselt number with the correlations of Ramanathan and Kumar (1991) and Rohsenow et al. (1998) for symmetric, isoflux, air-cooled channels.

with symmetrical heat flux wall conditions. For channel Rayleigh numbers from 10^3 to 10^6, i.e., the single plate regime, and three different aspect ratios ($A = 5$, 10, 15), the mean Nusselt number, which represent the inverse of the temperature, agreed to within 10%.

It must be noted that only one comparison with experimental work is presented herein because, to our best knowledge, no result was reported in the literature for local heat transfer and fluid flow property for a similar geometry. Some qualitative comparisons have been made with the results of Said and Krane (1990) who gave numerical and experimental results for a closely related problem: a semi-circular protrusion mounted on one side-wall of a vertical uniformly heated channel. Using a Cartesian grid in the present study, a semi-circular protrusion cannot be perfectly well simulated. Instead, a step-shape form was simulated, which is roughly semi-circular. A 42×102 grid was used for the total computational domain (channel and protrusion) with a maximum of 20 control volumes for the protrusion in the Y-direction and 30 in the X-direction. Variations of the local Nusselt number along the heated plates are given in Fig. 3. Very close agreement exists between the two studies; see Fig. 6 of Said and Krane (1990).

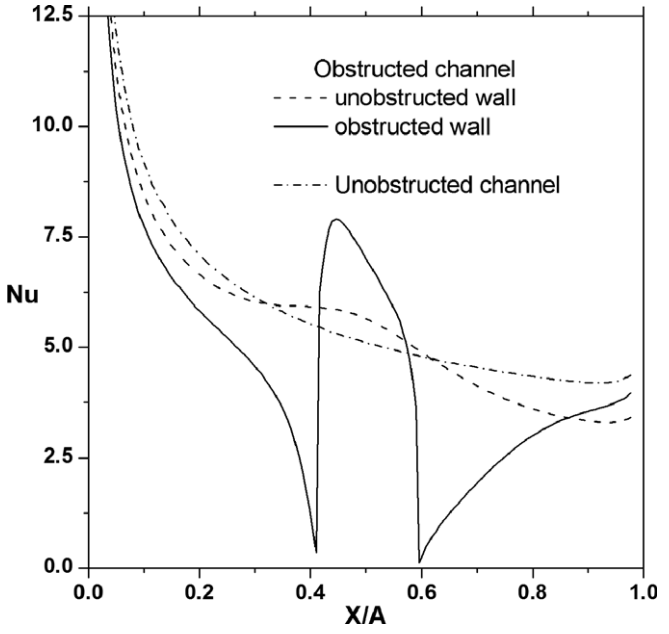

Fig. 3. Comparison with Said and Krane (1990) of the local Nusselt number along the heated plates for an isothermal obstructed channel, $A = 3.66$, dimensionless radius of the obstacle 0.33, $Ra = 2 \times 10^4$, $Pr = 0.72$.

A grid refinement study was conducted to determined adequacy of the mesh scheme (Table 1). Five non-uniform grid sizes of (NX, NY) elements in the X and Y-direction were evaluated for the test case. The mass flow rate, the dimensionless mean heat fluxes and the temperature of the module were computed. Differences between the value of these variables for the finest grid and the grid size 40×150 are around 1% while they reach 4% with the coarsest grid. Based on the grid refinement study, the grid size 40×150 was used for the model simulation. Details of the module usually required 10×30 control volumes while 4 are needed for each half-substrate thickness.

For most of the cases discussed in the present paper, the balance given by Eq. (9) was better than 1%. It must be noted that owing to the large channel Rayleigh numbers considered, the energy loss through the inlet by conduction (first integral term in the RHS of Eq. (9)) was always less than 1%. Upstream conduction can thus be assumed negligible and this justifies the restriction of the computational domain to the channel.

3. Results and discussion

Since the number of dimensionless parameters that influence the heat transfer and fluid flow characteristics is large, a comprehensive analysis of all possible combinations is not practical. Air at 1 atm and 20 °C was taken as the working medium, bakelite $\kappa_s = 1.4$ W/m−K ($\Lambda_s \approx 50$) as the typical board material, and silicon as the material of the protruding module, $\kappa_m = 148$ W/m−K ($\Lambda_m \approx 6000$). This choice of materials is one of the several combinations that could be used. However, printed circuit boards are commonly made in various composite materials. Therefore, the substrate-air conductivity ratio was varied from $\Lambda_s = 1$ to $\Lambda_s = 1000$. The channel aspect ratio was also fixed to $A = 5$. Thus to evaluate the effect of sub-

Table 1
Grid refinement results (multiple channels), $Ra^* = 2 \times 10^4$, $H = 1.0$, $W = 0.25$, $\Lambda_m = 6000$, $\Lambda_s = 50$, $S = 0.1$, $A = 5$, $Pr = 0.71$

NY	NX	$\dot{M}$	$\overline{Q}_{below}$	$\overline{Q}_m$	$\overline{Q}_{above}$	$\overline{Q}_{back}$	$\overline{\theta}_m$
30	100	43.35	0.1245	0.3203	0.0522	0.5030	0.0540
40	100	44.32	0.1181	0.3261	0.0497	0.5061	0.0524
40	150	44.93	0.1207	0.3256	0.0491	0.5044	0.0518
40	200	45.12	0.1207	0.3274	0.0484	0.5035	0.0517
50	200	44.86	0.1220	0.3254	0.0496	0.5030	0.0521

strate characteristics and module size, the numerical computations were carried out systematically by starting with a reference case for which the board thickness, thermal conductivity, module geometry and aspect ratio of the channel are $S = 0.1$, $\Lambda_s = 50$, $H = 1.0$, $W = 0.25$ and $A = 5$. The regions below and above the protruding source are referred to as the upstream and downstream regions, respectively in what follows. For comparison purpose, a channel with finite substrate and adiabatic condition on its back face is considered as the limiting configuration (Desrayaud et al., 2002).

3.1. General trends of the flow

Computations were performed for a channel Rayleigh number within the range $2 \times 10^3 \leqslant Ra^* \leqslant 2 \times 10^5$ which corresponds to heat dissipation in air, approximately from 0.03 W/cm^2 to 3 W/cm^2. These values are for a channel width of 2 cm, height of 10 cm and a substrate thickness of about 2 mm.

The streamfunction and isothermal patterns plotted in the present paper for various values of Ra^*, Λ_s, S and module width are reported in the legends with their maximum values. The maximum in streamline represents the dimensionless mass flow rate (except in the case of outlet flow recirculation). The module temperature is uniform for all of the computations discussed in what follows, owing to the large value of its thermal conductivity, and it is the maximum temperature reached inside the computational domain.

The effect of Ra^* on the fluid flow and temperature field is shown in Fig. 4 for $\Lambda_s = 50$. Substrate heat conduction re-directs a fraction of heat input upstream and downstream of the module but also across the substrate thickness to the adjacent channel. The high thermal conductivity of the substrate, relative to that of air, allows for thermal spreading to occur through the substrate with a substrate temperature gradient in the cross-stream direction very small. Whatever the channel Rayleigh number is, around 50% of heat input at the base of the module is transferred by conduction through the back face of the substrate and convected to air in the adjacent left channel. Table 2 gives the mean heat fluxes transferred to the fluid through the faces of the substrate (upstream, downstream, back) and of the module (bottom, vertical, top), the mean temperature of the module and the mass flow rate for various Ra^* and conductivity ratios. Mean heat fluxes are also shown on the plots of the isotherms (Fig. 4a–c) in per cent values. Therefore half of the input heat flux applied to the base of the module enters the fluid all along each faces of the substrate and this explains why the fluid is heated symmetrically along both faces of the substrate at the channel entrance; this is clearly observable at $Ra^* = 2 \times 10^3$ (Fig. 4a) for which the starting point for the boundary layers is at the wall channel entrance. Increasing the channel Rayleigh number from 2×10^3 to 2×10^5 increases the

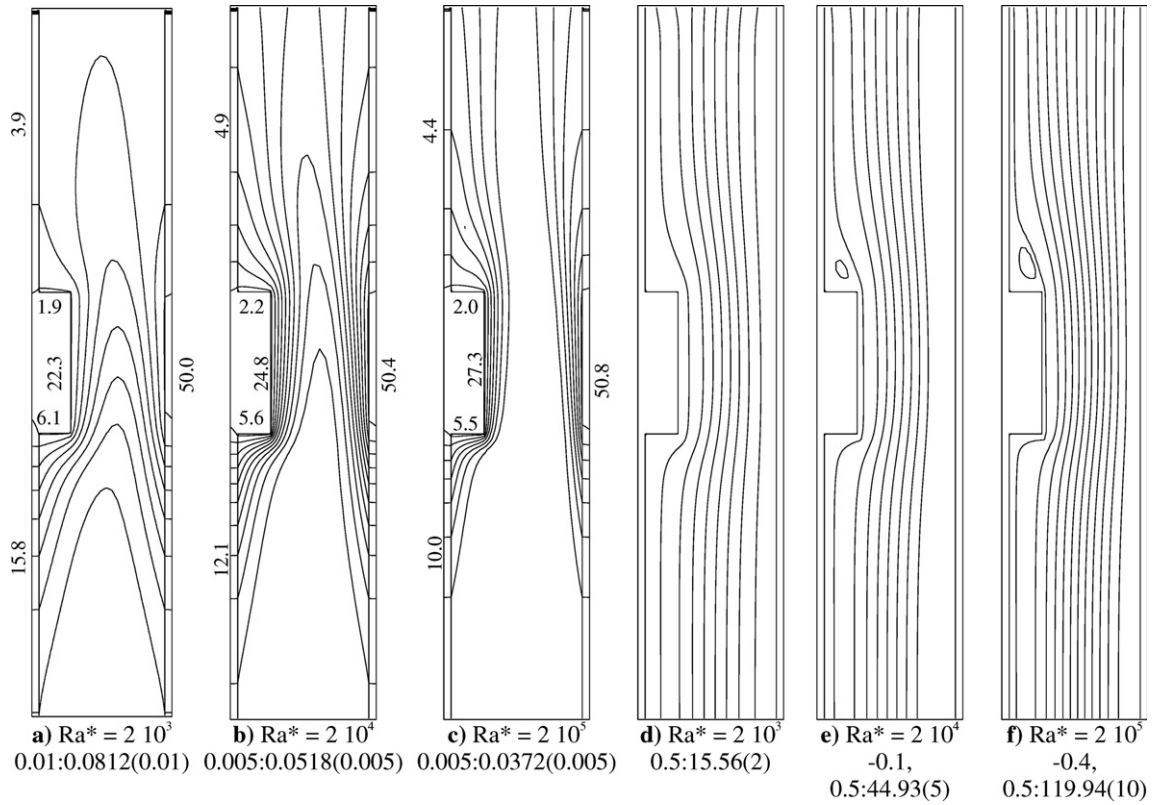

Fig. 4. Isotherms (a,b,c) and streamlines (d,e,f) for various values of the channel Rayleigh number for multiple channels, $\Lambda_s = 50$, $S = 0.1$, $H = 1$, $W = 0.25$, $A = 5$, $Pr = 0.71$ (data on the diagrams are % heat flux transferred through surfaces shown in Fig. 1).

Table 2
Characteristic values of the dimensionless heat fluxes (%), module temperature and mass flow rate for various channel Rayleigh numbers and substrate conductivity ratios for multiple channels, (lines in bold are for the single channel) $H = 1.0$, $W = 0.25$, $\Lambda_m = 6000$, $S = 0.1$, $A = 5$, $Pr = 0.71$

Ra^*	Λ_s	$\overline{Q}_{below}$	Module				$\overline{Q}_{above}$	$\overline{Q}_{front}$	$\overline{Q}_{back}$	$\overline{\theta}_m$	$\dot{M}$
			$\overline{Q}_{bottom}$	$\overline{Q}_{vertical}$	$\overline{Q}_{top}$	$\overline{Q}_m$					
2×10^3	1	−3.6	*17.0*	*43.5*	*6.1*	66.6	−4.1	58.9	41.1	0.1206	15.17
	50	15.8	*6.1*	*22.3*	*1.9*	30.3	3.9	50.0	50.0	0.0812	15.56
	1000	31.2	*1.8*	*10.2*	*0.7*	12.7	4.8	48.8	51.2	0.0599	15.80
	50	**37.5**	***7.7***	***35.6***	***3.8***	**47.1**	**15.4**	**100.0**	–	**0.1241**	**14.34**
2×10^4	1	−2.4	*15.1*	*47.5*	*6.0*	68.6	−6.0	60.2	39.8	0.0833	43.92
	10	3.4	*9.6*	*34.5*	*3.6*	47.7	0.3	51.4	48.6	0.0646	44.58
	50	12.1	*5.6*	*24.8*	*2.2*	32.6	4.9	49.6	50.4	0.0518	44.93
	100	16.0	*4.1*	*20.6*	*1.7*	26.4	6.7	49.1	50.9	0.0460	45.00
	1000	24.0	*1.9*	*11.9*	*1.2*	15.0	9.6	49.2	50.8	0.0342	44.80
	50	**33.0**	***7.7***	***38.8***	***3.9***	**50.4**	**16.6**	**100.0**	–	**0.0882**	**34.54**
2×10^5	1	−1.6	*13.7*	*52.3*	*5.5*	71.5	−6.4	63.6	36.4	0.0608	118.01
	50	10.0	*5.5*	*27.3*	*2.0*	34.8	4.4	49.2	50.8	0.0372	119.94
	1000	21.9	*1.8*	*13.0*	*0.8*	15.6	10.1	47.6	52.4	0.0235	118.81
	50	**30.6**	***8.0***	***41.2***	***3.8***	**53.0**	**16.4**	**100.0**	–	**0.0650**	**59.10**

convective heat transfer rate and less heat is conducted below the module through the front face (from 15.8% to 10.0%, respectively). Therefore, the distance from the inlet at which the fluid becomes pre-heated increases (Fig. 4b and c). Although an equal amount of heat is transferred by the two faces to the fluid, the heating symmetry of the flow is destroyed by the protruding module. On the front face of the substrate, the main part of the heat is conducted through the module (from 30.3% at $Ra^* = 2\times10^3$ to 34.8% at $Ra^* = 2\times10^5$) and the largest temperature gradient occurs in the fluid near the module. Separate thermal boundary layers are only observed at the highest value of the channel Rayleigh number, $Ra^* = 2\times10^5$ (Fig. 4c). When increasing Ra^* the mass flow rate through the chan-

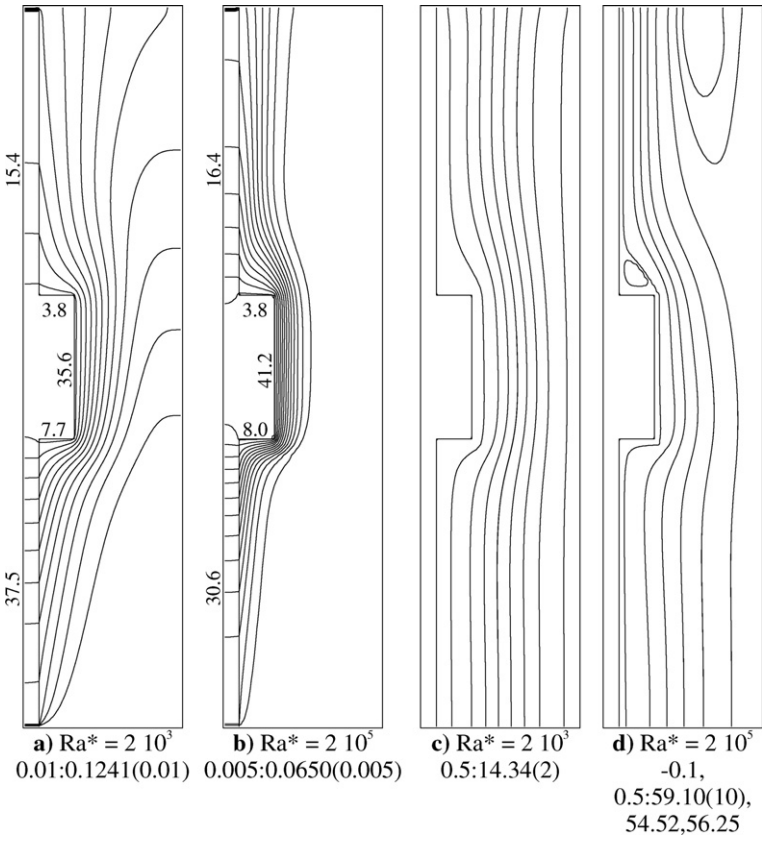

Fig. 5. Isotherms (a,b) and streamlines (c,d) for various values of the channel Rayleigh number for a single channel, $\Lambda_s = 50$, $S = 0.1$, $H = 1$, $W = 0.25$, $A = 5$, $Pr = 0.71$ (data on the diagrams are % heat flux transferred through surfaces shown in Fig. 1).

nel increases and air starts to follow the module contours more closely. A stagnant zone exists just below the module but no eddy was detected, even at $Ra^* = 2 \times 10^3$. The shear force of the main stream is indeed unable to promote a counter-clockwise eddy and the streamlines are closer and closer to the inside corner when increasing Ra^*. The streamlines show that the main difference between Fig. 4d–f is the occurrence of a weak secondary counter-clockwise vortex at $Ra^* = 2 \times 10^4$ resulting from the separation of the main stream at the trailing edge of the module and from the viscous entrainment of the fluid flow.

Fig. 5 displays the dimensionless isotherms and streamlines for two different channel Rayleigh numbers but for the limiting case of an adiabatic boundary condition on the back face of the substrate, i.e., the single channel limit. It can be noticed that the entire thickness of the substrate is shown on the left side of the channel (contrarily to multiple channels for which half of the substrate thickness is shown on the left side, the other half being on the right side). Since the buoyancy force acts along one face of the channel only, the streamlines are concentrated near the left wall. A recirculation cell is observed at the outlet for $Ra^* = 2 \times 10^5$, close to the adiabatic shrouding plate, in order to supply air for the growth of the boundary layer. At $Ra^* = 2 \times 10^3$ (and at 2×10^4 not shown here) no fluid penetration occurs through the outlet. Obviously, the module temperature is systematically much higher for the single channel case than for multiple channels. Concerning the mass flow rate, the amounts are almost the same in both cases at $Ra^* = 2 \times 10^3 (\dot{M} \approx 15)$ while it is much lower in the case of single channel for $Ra^* = 2 \times 10^5 (\dot{M} = 59.10$ for single channel and 119.94 for multiple channels). An almost equal repartition of the heat transfer through both faces of the substrate explains the occurrence of a boundary layer along both walls in multiple channels and, consequently, the increases in mass flow rate, provided Ra^* is large enough.

Fig. 6a, showing the temperature profile along the substrate, evidences these trends. The non-dimensional temperatures are smaller for higher values of Ra^* because θ is inversely proportional to the input heat flux. Small differences between back and front profiles for multiple channels are seen only near the edge of the module owing to the low thermal resistance of the substrate. This almost identical profile on both faces of the substrate is also indicated by the nearly horizontal isotherms in the solid region shown in Fig. 4a–c. On the other hand, the large differences in module temperatures between single and multiple channels demonstrate the importance of the heat transfer through the back face. The increase in the heat transfer surface for multiple channel configurations (which is roughly doubled) is thus of crucial importance in cooling the module.

The variations of the dimensionless local heat flux Q at the solid–fluid interface (Eq. (8)) are shown in Fig. 6b as a function of the ζ-coordinate which is a dimensionless contour distance along the solid–fluid interface, from the bottom to the top of the channel. Inside and outside corner locations are shown by dashed lines. Five zones have been defined on the front face of the solid, the surface below the module (upstream substrate, $0 \leqslant \zeta \leqslant 2$), the surface of the module which is divided as bottom ($2 \leqslant \zeta \leqslant 2.25$), vertically ($2.25 \leqslant \zeta \leqslant 3.25$) and top ($3.25 \leqslant \zeta \leqslant 3.5$) oriented module faces, and the surface above the module (downstream substrate, $3.5 \leqslant \zeta \leqslant 5.5$).

The dimensionless heat flux first increases due to the increase of the axial substrate temperature (Fig. 6a) whatever Ra^* is, and approaches zero (and can be negative) at the inside corners of the module at $\zeta = 2$ because the solid–fluid thermal resistance is increased by the stagnant conditions. At the bottom face of the module, the heat flux increases sharply to reach a maximum at the external bottom corner ($\zeta = 2.25$) due to the boundary layer thinning upon turning the corner. The same behavior is observed at the trailing edge with a lower maximum ($\zeta = 3.25$). The decrease of the heat flux from the leading to the trailing edge of the module arises from the thickening of the boundary layer along the vertical surface. This part of the channel behaves like a symmetrically heated channel at fixed temperatures. At the top surface of the module,

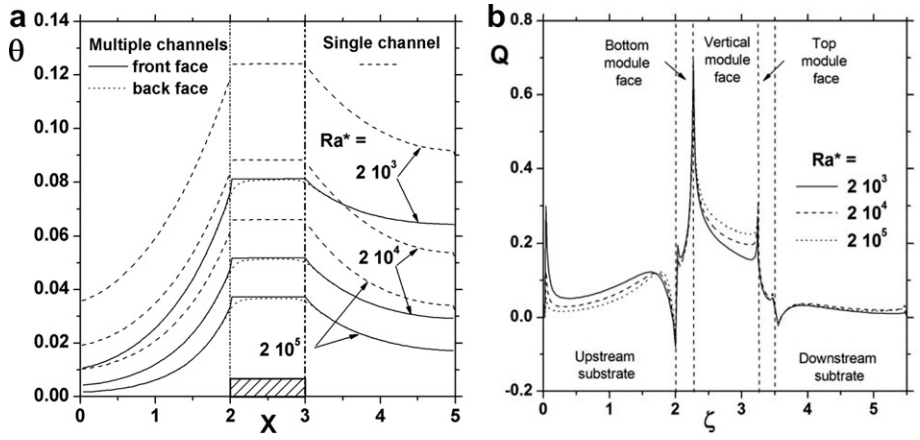

Fig. 6. Temperature (a) and local heat flux (b) profiles for various values of the Rayleigh number, $\Lambda_s = 50$, $S = 0.1$, $H = 1$, $W = 0.25$, $A = 5$, $Pr = 0.71$. (a) Temperature profile along the front and back faces of the substrate. (b) Local heat flux profile along the solid–fluid front interface of the substrate.

the heat flux approaches zero anew. Above the module, the small maxima characterize the main flow re-attachment on the substrate surface. The heat flux entering the fluid then decreases continuously, owing to the decrease of the conduction inside the substrate (Fig. 6a).

Similar local heat flux trends are observed whatever Ra^* is, but with different magnitude (Fig. 6b). At $Ra^* = 2 \times 10^3$, significant energy enters the fluid at the substrate–fluid interface below the module due to comparatively weak convection from the module surface and a favorable conduction path from the module, through the substrate to the fluid. The percentage of the heat flux extracted below the module by the fluid motion decreases with increasing channel Rayleigh number. On the other hand, the convective motion being more vigorous, the heat extracted at the module, especially at its vertical face, becomes higher. No significant differences are seen at the horizontal faces of the module (stagnant zones) or between the heat flux profiles above the module. In comparison, the heat flux at the solid–fluid back interface of the substrate (not shown here) is considerably smoothed because of the vertical heat conduction within the substrate.

3.2. Effect of substrate characteristics

3.2.1. Thermal conductivity, Λ_s

The effect of substrate thermal conductivity was determined with Ra^* fixed at $Ra^* = 2 \times 10^4$ and thermal conductivity of the module equal to that of silicon ($\Lambda_m = 6000$). The conductivity ratio was varied in the range $1 \leqslant \Lambda_s \leqslant 1000$. Following the usual fin approximate analysis, the thermal resistance of the downstream (or upstream) substrate may be approximated as:

$$R_s \approx \frac{1}{(\ell h_s \kappa_s s)^{0.5}}. \tag{10}$$

The effect of Λ_s on the dimensionless temperature fields is displayed in Fig. 7a–b. For the sake of brevity, streamlines are not shown here because they resemble those presented in Fig. 4e for $\Lambda_s = 50$. The substrate thermal conductivity has a very small effect on both mass flow rate (variation less than 2% around a mean value $\dot{M} = 44.6$, see Table 2) and structure of the flow. At the lowest value of Λ_s the region below the module is almost isothermal at the inlet air temperature (see also Fig. 8a) and the isotherms are concentrated close to the heated module. A wall-plume with characteristic cap isotherm shape forms above the module and the heated air rises along the substrate and is entrained into the plume. Increasing the substrate thermal conductivity significantly affects the heat transfer from the module and along the substrate in upstream and downstream directions. A thermal boundary layer forms at the inlet and thickens when the flow proceeds downstream. For very large Λ_s the substrate conduction dominates and the problem is similar to that of an isothermal wall (Figs. 7b and 8a).

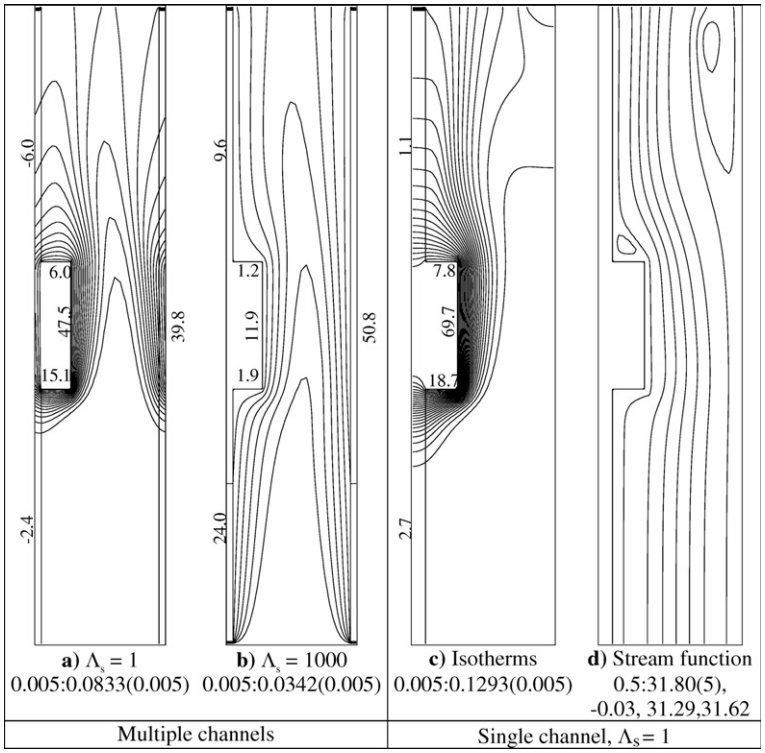

Fig. 7. Temperature field (a,b) for various values of the substrate-air conductivity ratio Λ_s for multiple channels. Isotherms (c) and streamlines (d) for a single channel with $\Lambda_s = 1$. $Ra^* = 2 \times 10^4$, $S = 0.1$, $H = 1$, $W = 0.25$, $A = 5$, $Pr = 0.71$ (data on the diagrams are % heat flux transferred through surfaces shown in Fig. 1).

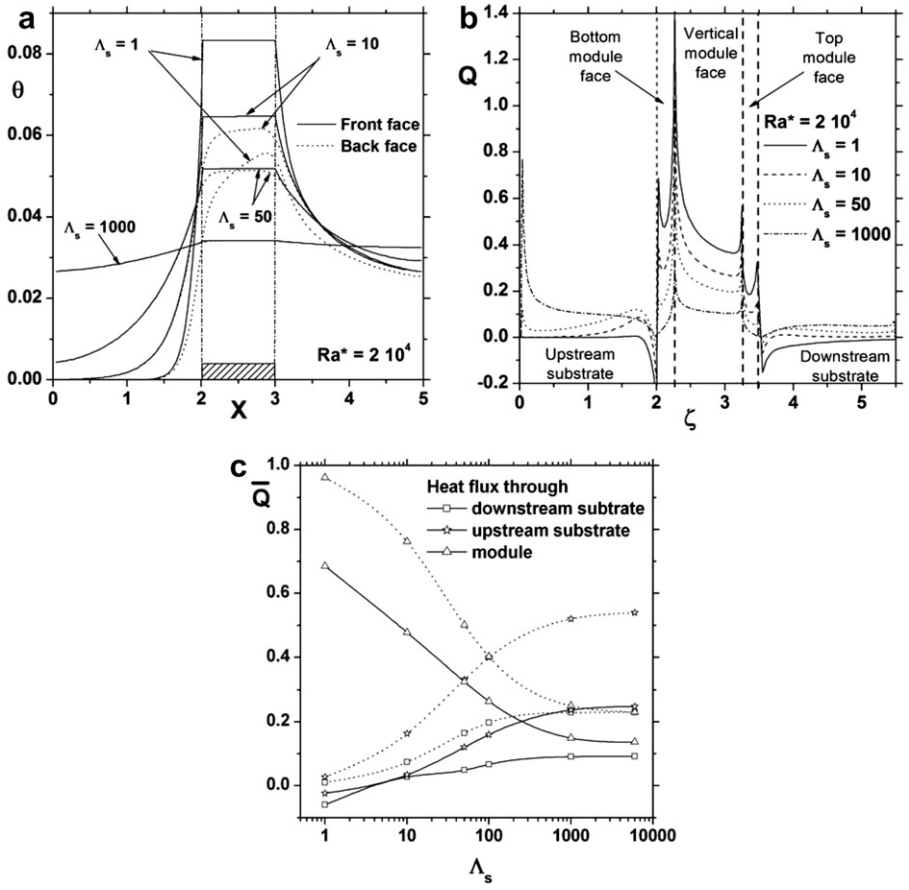

Fig. 8. Temperature (a), local heat flux profiles (b) and fractions of input heat flux (c) for various values of the substrate-air conductivity ratios, $Ra^* = 2 \times 10^4$, $S = 0.1$, $H = 1$, $W = 0.25$, $A = 5$, $Pr = 0.71$. (a) Temperature profile along the front face of the substrate. (b) Local heat flux profile along the solid–fluid front interface of the substrate. (c) Fractions of the mean heat flux through the front face of the substrate and the module surface, (—) Multiple channels, (- - -) Single channel.

Fig. 7c and d presents the temperature and stream function fields in the case of single channel for $\Lambda_s = 1$. The isotherms (Fig. 7c) clearly indicate that the module temperature is higher than that found for multiple channels (Fig. 7a) and that the thermal field spreads far away in the upstream direction. Contrarily to what has been found in the case of the multiple channels, the structure of the flow field is significantly affected by the substrate thermal conductivity since a recirculation region is present along the shrouding plate for $\Lambda_s = 1$ (Fig. 7d). This recirculation disappears when increasing the conductivity ratio because the input heat flux at the base of the module spreads along all the substrate as for multiple channels.

Interesting heat transfer trends are also revealed when the dimensionless solid surface temperatures are examined at $Ra^* = 2 \times 10^4$ for various conductivity ratios in Fig. 8a. At a low value of the substrate conductivity ($\Lambda_s = 1$), a small amount of heat is spread into the substrate by conduction and the temperature of the substrate below the module is close to the inlet air temperature. Increases in Λ_s lead to increases in pre-heating of air before it reaches the module. Temperature profiles on the back face of the substrate for multiple channels are also shown in Fig. 8a (dotted lines). Large differences between front and back temperature profiles appear for the lowest value of the substrate conductivity ($\Lambda_s = 1$), especially close to the module location, and a large asymmetry is seen with a maximum near the trailing edge of the module ($X = 3$). The module and substrate thermal conductivity being of the same order of magnitude, the heat source begins to lose its thermal identity and becomes more difficult to locate.

Fig. 8b gives the dimensionless local heat flux Q from the front faces to the fluid. Profiles are very similar to those presented in Fig. 6b. While no heat is transferred below the module at $\Lambda_s = 1$ the heat transfer increases slightly along the upstream substrate for $\Lambda_s = 10$ and 50. An inverse trend is observed for $\Lambda_s = 1000$ since the heat transfer decreases from the channel inlet to the module, as for a channel heated at constant temperature for which the boundary layer thickens along the wall.

Shown in Fig. 8c are the fractions of heat flux removed by convection from the module and from the upstream and downstream front faces of the substrate for multiple and single channels as a function of Λ_s. When increasing the substrate conductivity, the heat removal from the module sharply decreases because the substrate acts as a heat sink,

reducing the module temperature (Fig. 8a). It should be noted that the heat transferred to the substrate is always higher below the module than above, with an increasing difference when increasing the conductivity ratio. This comes from the bulk temperature of air increasing when the flow proceeds downstream, especially at the module, the temperature increase being reinforced by the narrowing of the by-pass region.

3.2.2. Substrate thickness

A set of calculations was performed for $Ra^* = 2 \times 10^4$ and for various substrate thickness in the range $0.05 \leqslant S \leqslant 0.35$. The effect of S on the dimensionless temperature fields is shown in Fig. 9a and b for two different values of S. The mass flow rate is almost constant, varying from 44.79 for $S = 0.05$ to 55.01 for $S = 0.35$. The thermal resistance of the substrate decreases with S as shown by Eq. (10) and hence the thermal spreading in the substrate increases. As a consequence, the fluid is more pre-heated before having reached the module, all the more so since the substrate is thick (Fig. 9b). As is confirmed by Eq. (10), the heat conducted through the substrate is not proportional to its thickness but increases sharply from $S = 0.05$ to $S = 0.3$ while only a small increase is noted for $S = 0.35$. Isotherms given for a single channel with $S = 0.05$ (Fig. 9c and d) show that the module temperature is greater (0.0984 for a single channel, 0.0567 for multiple channels) because of the reduced heat transfer area due to the adiabatic back face. Although thermal spreading extended more largely in the upstream substrate as can be seen comparing Fig. 9a and c, it does not compensate the fact that only one face of the substrate can convect heat to the fluid.

3.3. Effect of module width

Increasing the module width should lead to a decrease in the temperature level due to the reduction in power density. However, the reduction of the by-pass region, and consequently of the mass flow rate, produces an opposite effect for channel flows. There is a competition between the exposed surface to the fluid flow and the reduction in the mass flow rate due to the restriction of the opening.

Fig. 10 shows a comparison of the isotherms and streamlines for two different widths of the module for multiple channels. As can be seen, the streamlines and isotherm patterns are slightly altered in the vicinity of the module at the lowest width, i.e., $W = 0.125$, and are similar to those found in a symmetrically heated smooth channel. The influence of the module width is very weak on the amount of heat convected through the back face of the substrate. Because of the high conductivity, the module has a low thermal resistance and half of the input heat flux is transferred to the back face of the substrate whatever the width is. The mass flow rate, given in the legend of Fig. 10 as the maximum value of the stream function, shows a substantial decrease with W ($\dot{M} = 48.59$ for $W = 0.125$, $\dot{M} = 14.66$ for $W = 0.75$). The counter-clockwise eddy found for $W = 0.25$ (Fig. 4e) on the top face of the module strengthens in size as the width of the module increases. Therefore,

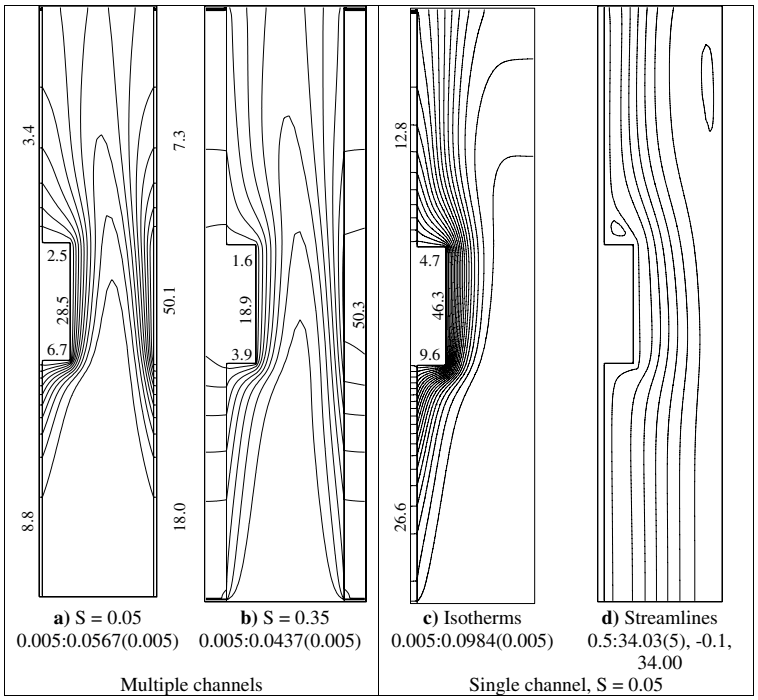

Fig. 9. Isotherms (a,b) for various values of the thickness of the substrate S for multiple channels. Isotherms (c) and streamlines (d) for a single channel with $S = 0.05$. $Ra^* = 2 \times 10^4$, $\Lambda_s = 50$, $H = 1$, $W = 0.25$, $A = 5$, $Pr = 0.71$ (data on the diagrams are % heat flux transferred through surfaces shown in Fig. 1).

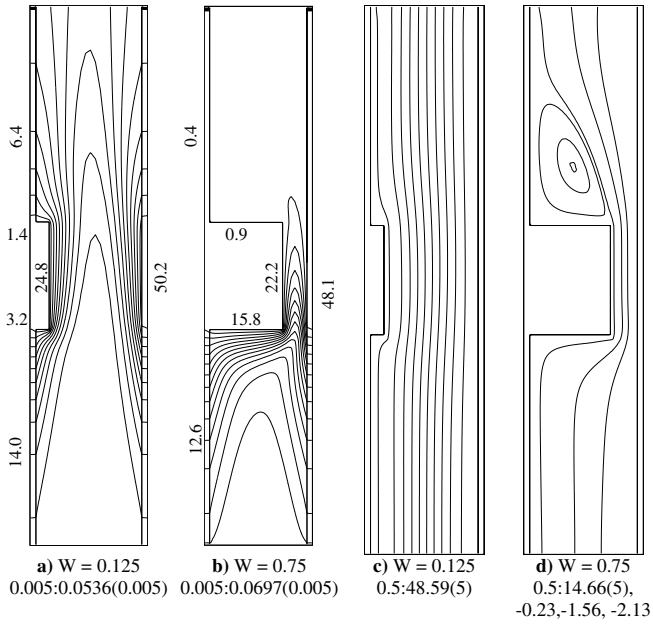

Fig. 10. Isotherms (a,b) and streamlines (c,d) for various values of the module width for multiple channels, $Ra^* = 2\times10^4$, $S = 0.1$, $H = 1$, $\Lambda_s = 50$, $A = 5$, $Pr = 0.71$ (data on the diagrams are % heat flux transferred through surfaces shown in Fig. 1).

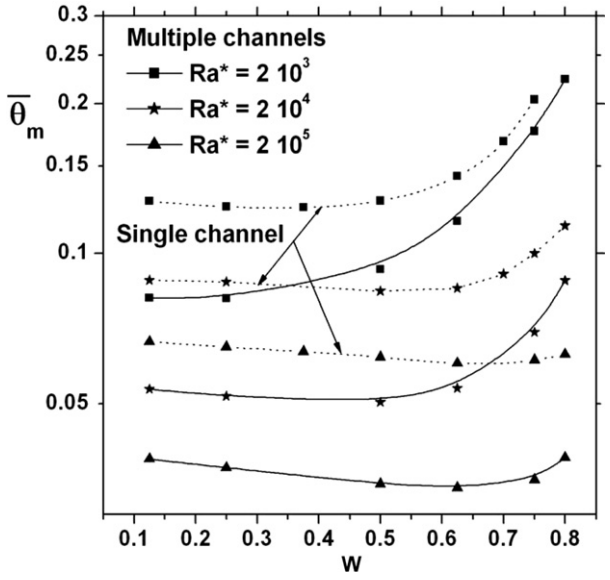

Fig. 11. Module mean temperature for three values of the channel Rayleigh number versus the width of the module, $\Lambda_s = 50$, $S = 0.1$, $H = 1$, $A = 5$, $Pr = 0.71$.

the reattachment of the main flow far downstream of the module inhibits the heat transfer from the substrate at the close downstream region as well as at the top face of the module.

Reliability considerations dictate that the module temperature should be maintained below a safe functional limit. Thermal resistance is often associated with heat sink in electronic systems representing the induced temperature drop for a fixed energy flux. The thermal resistance of the module is defined as,

$$R_m = (T_m - T_0)/q''h$$

or in dimensionless form

$$R_m \kappa_a = \bar{\theta}_m / H.$$

Fig. 11 shows the variation of the mean module temperature versus its width for a fixed height, $H = 1$, and for three different Ra^*-values. It should be noted that $\bar{\theta}_m$ represents the thermal resistance per unit length between the module and the ambient fluid. As a consequence of the competition between the increase of the heat transfer surface and the reduction in the mass flow rate, there is an optimum width at which the heat flux through the module is maximum and the module temperature minimum at high Ra^*. For $Ra^* = 2\times10^4$ (2×10^5, respectively), this optimum is about $W = 0.50$ (resp., 0.625) for multiple channels. On the other hand, the mass flow rate is small and convection plays a minor role for $Ra^* \leqslant 2\times10^3$. Moreover, the occurrence of an eddy above the top face of the module reduces the heat transfer rate there. This is of great importance at low values of Ra^* (2×10^3) at which conduction within the fluid is an important heat transfer mechanism, and explains why an increase in the module temperature occurs immediately when the module width is increased. In the single channel configuration, the trend of the curves are almost the same with the module temperature always greater than in the case of multiple channels, the heat spreading being bound by the adiabatic back face of the substrate.

4. Conclusions

A parametric study for 2D-conjugate heat transfer from protruding heat modules in vertical channels was numerically conducted to determine the effects of channel Rayleigh number, substrate/fluid thermal conductivity and module dimensions. The system simulates air-cooling passages in a stack of printed circuit boards. The computational domain was restricted by the use of periodic conditions inside the substrate.

Heat from the module is removed in part by natural airflow at the module while the rest is conducted to the substrate before being dissipated in the two adjacent channels. Increasing the Rayleigh number increases the buoyancy force, and the mass flow rate intensifies. More heat is then extracted at the vertical face of the module. It must be noted that for the given heat conductivity ratio, $\Lambda_s = 50$, the percentage of heat extracted through the back face (around 50%) is insensitive to the channel Rayleigh number variation.

- When increasing the thermal conductivity of the substrate, the heat flux distribution between the module and the upstream and downstream front faces of the substrate changes significantly. As a consequence, the module temperature decreases. However, the heat

transferred by conduction to the back face of the substrate and the mass flow rate through the channel are only slightly modified.
- Increasing the thickness of the substrate enhances the fin effects. Consequently, the module temperature decreases.
- For $Ra^* \geqslant 2 \times 10^3$, the mass flow rate reduction due to a larger module width is counterbalanced by the increase of the heat transfer surface. Therefore, an optimum in plate spacing could be achieved according to the module width.

It is inappropriate to decouple conductive heat transfer within the substrate and natural convection in the channel. The use of isothermal or isoflux boundary conditions at the channel surfaces does not properly represent the heat transfer characteristics.

Acknowledgement

The authors gratefully acknowledge the support of this work by a grant No. 031265 from the IDRIS-Computer Center (French National Institute for Advances in Scientific Computations). M. Gulino assisted part in the numerical calculations.

References

Behnia, M., Dehghan, A.A., Mishima, H., Nakayama, W., 1998. A numerical study of natural convection immersion cooling of multiple heat sources in parallel interacting open-top cavities. Int. J. Heat Mass Transfer 41 (4–5), 797–808.

Davalath, J., Bayazitoglu, Y., 1987. Forced convection cooling across rectangular blocks. J. Heat Transfer 109, 321–328.

Desrayaud, G., Fichera, A., 2003. On natural convective heat transfer in vertical channels with a single surface mounted heat-flux module. J. Heat Transfer 125, 734–739.

Desrayaud, G., Fichera, A., Lauriat, G., 2002. Conjugate heat transfer from a substrate-mounted protruding heat source in air-cooled vertical channels. In: Proceedings of the 12th Int. Heat Transfer Conf., vol. 2, pp. 771–776.

Floryan, J.M., Novak, M., 1995. Free convection heat transfer in multiple vertical channels. Int. J. Heat Fluid Flow 16, 244–253.

Furukawa, T., Yang, W.-J., 2003. Thermal-fluid flow in parallel boards with generating blocks. Int. J. Heat Mass Transfer 46, 5005–5015.

Fujii, M., Gima, S., Tomimura, T., Zhang, X., 1996. Natural convection to air from an array of vertical parallel plates with discrete and protruding heat sources. Int. J. Heat Fluid Flow 17 (5), 483–490.

Fujii, M., Tomimura, T., Zhang, X., Gima, S., 1994. Natural convection from an array of vertical parallel plates. In: Proc. 10th Int. Heat Transfer Conf., vol. 7, pp. 49–54.

Habchi, S., Acharya, S., 1986. Laminar mixed convection in a partially blocked, vertical channel. Int. J. Heat Mass Transfer 29, 1711–1722.

Hung, Y.H., Shiau, W.M., 1988. Local steady-state natural convection heat transfer in vertical parallel plates with a two-dimensional rectangular rib. Int. J. Heat Mass Transfer 31, 1279–1288.

Kim, S.H., Anand, N.K., 1994. Laminar developing flow and heat transfer between a series of parallel plates with surface mounted discrete heat sources. Int. J. Heat Mass Transfer 37 (15), 2231–2244.

Kim, S.H., Anand, N.K., Fletcher, L.S., 1991. Free convection between series of vertical parallel plates with embedded line heat sources. J. Heat Transfer 113, 108–115.

Kim, S.Y., Sung, H.J., Hyun, J.M., 1992. Mixed convection from multiple-layered boards with cross-streamwise periodic boundary conditions. Int. J. Heat Mass Transfer 35, 2941–2952.

Kwak, C.E., Song, T.H., 1998. Experimental and numerical study on natural convection from vertical plates with horizontal rectangular grooves. Int. J. Heat Mass Transfer 41, 2517–2528.

Lin, T.-Y., Hsieh, S.-S., 1990. Natural convection of opposing/assisting flows in vertical channels with asymmetrically discrete heated ribs. Int. J. Heat Mass Transfer 33, 2295–2309.

Marcondes, F., Maliska, C.R., 1999. Treatment of the inlet boundary conditions in natural-convection flows in open-ended channels. Num. Heat Transfer 35B, 317–345.

Mallison, G.D., de Vahl Davis, G., 1973. The method of false transient for the solution of coupled elliptic equations. J. Comp. Phys. 12, 435–461.

Patankar, S.V., 1980. Numerical Heat Transfer and Fluid Flow. Hemisphere/Mc Graw-Hill, Washington.

Ramanathan, S., Kumar, R., 1991. Correlations for natural convection between heated vertical plates. J. Heat Transfer 113, 97–107.

Rohsenow, W.M., Hartnett, J.P., Cho, Y.I. (Eds.), 1998. Handbook of Heat Transfer. McGraw-Hill, New York.

Said, S.A.M., Krane, R.J., 1990. An analytical and experimental investigation of natural convection heat transfer in vertical channels with a single obstruction. Int. J. Heat Mass Transfer 3, 1121–1134.

Sathe, S., Sammakia, B., 1998. A review of recent developments in some practical aspects of air-cooled electronic packages. J. Heat Transfer 120, 830–839.

Tanda, G., 1997. Natural convection heat transfer in vertical channels with and without transverse square ribs. Int. J. Heat Mass Transfer 40, 2173–2185.

Wirtz, R.A., Stutzman, R.J., 1982. Experiments on free convection between vertical plates with symmetric heating. J. Heat Transfer 104, 501–507.

Zamora, B., Hernandez, J., 1997. Influence of variable property effects on natural convection flows in asymmetrically-heated vertical channels. Int. Comm. Heat Mass Transfer 24, 1153–1162.